DE-FC26-99FT40054--01

#01

Oxygen Transport Ceramic Membranes

Quarterly Report

July -- September 2000

By:

Dr. Sukumar Bandopadhyay
and
Dr. Nagendra Nagabhushana

School of Mineral Engineering
University of Alaska Fairbanks

Issued: October 2000

DOE Award # DE-FC26-99FT400054

40054 R01

University of Alaska Fairbanks
School of Mineral Engineering
Brooks 209
Fairbanks, AK 99775

DISCLAIMER

Executive Summary

Conversion of natural gas to liquid fuels and chemicals is a major goal for the Nation as it enters the 21st Century. Technically robust and economically viable processes are needed to capture the value of the vast reserves of natural gas on Alaska's North Slope, and wean the Nation from dependence on foreign petroleum sources. Technologies that are emerging to fulfill this need are all based syngas as an intermediate. Syngas (a mixture of hydrogen and carbon monoxide) is a fundamental building block from which chemicals and fuels can be derived. Lower cost syngas translates directly into more cost-competitive fuels and chemicals.

The currently practiced commercial technology for making syngas is either steam methane reforming (SMR) or a two-step process involving cryogenic oxygen separation followed by natural gas partial oxidation (POX). These high-energy, capital-intensive processes do not always produce syngas at a cost that makes its derivatives competitive with current petroleum-based fuels and chemicals.

In the mid 80's BP invented a radically new technology concept that will have a major economic and energy efficiency impact on the conversion of natural gas to liquid fuels, hydrogen, and chemicals.[1] This technology, called Electropox, integrates oxygen separation with the oxidation and steam reforming of natural gas into a single process to produce syngas with an economic advantage of 30 to 50 percent over conventional technologies.[2]

The Electropox process uses novel and proprietary solid metal oxide ceramic oxygen transport membranes [OTMs], which selectively conduct both oxide ions and electrons through their lattice structure at elevated temperatures.[3] Under the influence of an oxygen partial pressure gradient,

---

[1]Mazanec, T. J.; Cable, T. L.; Frye, J. G., Jr.; US 4,793,904, 27 Dec 1988, assigned to The Standard Oil Company (now BP America), Mazanec, T. J.; Cable, T. L.; US 4,802,958, 7 Feb 1989, assigned to the Standard Oil Co. (now BP America), Cable, T. L.; Mazanec, T. J.; Frye, J. G., Jr.; European Patent Application 0399833, 24 May 1990, published 28 November 1990.

[2]Bredesen, R.; Sogge, J.; "A Technical and Economic Assessment of Membrane Reactors for Hydrogen and Syngas Production" presented at Seminar on the Ecol. Applic. of Innovative Membrane Technology in the Chemical Industry", Cetraro, Calabria, Italy, 1-4 May 1996.

[3]Mazanec, T.J., *Interface*, 1996; Mazanec, T.J., *Solid State Ionics*, 70/71, 1994 11-19; "Electropox: BP's Novel Oxidation Technology", T.J. Mazanec, pp 212-225, in "The Role of Oxygen in Improving Chemical Processes", M. Fetizon and W.J. Thomas, eds, Royal Society of Chemistry, London, 1993; "Electropox: BP's Novel Oxidation Technology", T.J. Mazanec, pp 85-96, in "The Activation of Dioxygen and Homogeneous Catalytic Oxidation", D.H.R. Barton, A. E. Martell, D.T. Sawyer, eds, Plenum Press, New York, 1993; "Electrocatalytic Cells for Chemical Reaction", T.J. Mazanec, T.L. Cable, J.G. Frye, Jr.; Prep Petrol Div ACS, San Fran, 1992 *37*, 135-146; T.J. Mazanec, T.L. Cable, J.G. Frye, Jr.; *Solid State Ionics*, 1992, 53-56, 111-118.

oxygen ions move through the dense, nonporous membrane lattice at high rates with 100 percent selectivity. Transported oxygen reacts with natural gas on the fuel side of the ceramic membrane in the presence of a catalyst to produce syngas.

In 1997 BP entered into an OTM Alliance with Praxair, Amoco, Statoil and Sasol to advance the Electropox technology in an industrially sponsored development program. These five companies have been joined by Phillips Petroleum and now are carrying out a multi-year $40+ million program to develop and commercialize the technology. The program targets materials, manufacturing and engineering development issues and culminates in the operation of semi-works and demonstration scale prototype units.

The Electropox process represents a truly revolutionary technology for conversion of natural gas to synthesis gas not only because it combines the three separate unit operations of oxygen separation, methane oxidation and methane steam reforming into a single step, but also because it employs a chemically active ceramic material in a fundamentally new way. On numerous fronts the commercialization of Electropox demands solutions to problems that have never before been accomplished. Basic problems in materials and catalysts, membrane fabrication, model development, and reactor engineering all need solutions to achieve commercial success.

Six important issues have been selected as needing understanding on a fundamental level at which the applied Alliance program cannot achieve the breadth and depth of understanding needed for rapid advancement. These issues include

1. Oxygen diffusion kinetics (University of Houston)
2. Grain structure and atomic segregation (University of Illinois - Chicago)
3. Phase stability and stress development (University of Missouri - Rolla)
4. Mechanical property evaluation in thermal and chemical stress fields (University of Alaska Fairbanks)
5. Graded ceramic/metal seals (Massachusetts Institute of Technology)

Statement of Work

Task 1 Design, fabricate and evaluate ceramic to metal seals based on graded ceramic powder / metal braze joints.

Task 2 Evaluate the effect of defect configuration on ceramic membrane conductivity and long term chemical and structural stability.

Task 3 Determine materials mechanical properties under conditions of high temperatures and reactive atmospheres.

Task 4 Evaluate phase stability and thermal expansion of candidate perovskite membranes and develop techniques to support these materials on porous metal structures.

Task 5 Assess the microstructure of membrane materials to evaluate the effects of vacancy-impurity association, defect clusters, and vacancy-dopant association on the membrane performance and stability.

Task 6 Measure kinetics of oxygen uptake and transport in ceramic membrane materials under commercially relevant conditions using isotope labeling techniques.

This is the third quarterly report on oxygen Transport Ceramic Membranes. In the following, the report describes the progress made by our university partners in Tasks 1 through 6, experimental apparatus that was designed and built for various tasks of this project, thermodynamic calculations, where applicable and work planned for the future

Task 1 & 2 Development of Ceramic Membrane/Metal Joints

Prof. Thomas W. Eagar, Dr Harold R Larson,
Mr Raymundo Arroyave and Ms Jocelyn L. Wiese

ABSTRACT

This is the fourth quarterly report on a new study to develop a ceramic membrane/metal joint. The first experiments using the La-Sr-Fe-O ceramic are reported. Some of the analysis performed on the samples obtained are commented upon. A set of experiments to characterize the mechanical strength and thermal fatigue properties of the joints has been designed and begun. Finite element models of joints used to model residual stresses are described.

Preliminary experiments using La-Sr-Fe-O discs.

Several experiments have been performed using ceramic oxygen membrane ($La_{.6}Sr_{.4}FeO_3$) and Haynes 230® discs. The first studies, using "conventional" reactive brazing alloys (with titanium or zirconium additions) showed excessive reactivity between the ceramic membrane and the braze. It is suspected that extensive decomposition of the membrane takes place due to the reaction between the reactive element dissolved in the braze and the oxygen from the ceramic.

Because of the extensive reactivity exhibited by titanium/zirconium-containing alloys, other liquid phase joining techniques were surveyed. Thanks to some preliminary experiments, it has been found that conventional amorphous nickel-based alloys are capable of wetting the ceramic surface. Nickel-based brazing alloys also have the advantage of having relatively low brazing temperatures (1090 C). This brazing temperature is achieved by the additions of boron or silicon to the nickel-based alloy.

Additionally, the fact that boron can be diffused away from the braze, providing that the joint is held at high temperature for long enough time, constitutes an additional advantage since it would be possible (in theory) to braze at one temperature, while operating at a higher one.

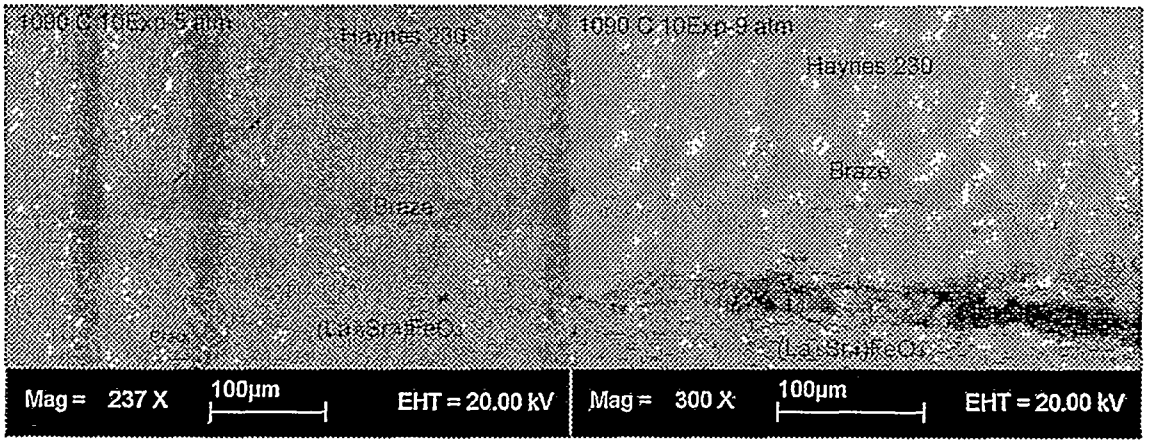

Figure 1 Ceramic membrane/braze/super alloy joint

Despite the good wettability behavior of these brazing alloys two important phenomena have been observed:

- Circumferential cracks, parallel to the ceramic/metal interface, appear to form after the joints are created. Preliminary evidence suggests that this cracking might be reduced if the brazing process takes place under higher oxygen partial pressure environments. In fact, it has been observed that this cracking appears to be minimized when the oxygen partial pressure is above 10^{-5} atm (See Figure 1 and Figure 2). Further research has to be done to verify this preliminary result.

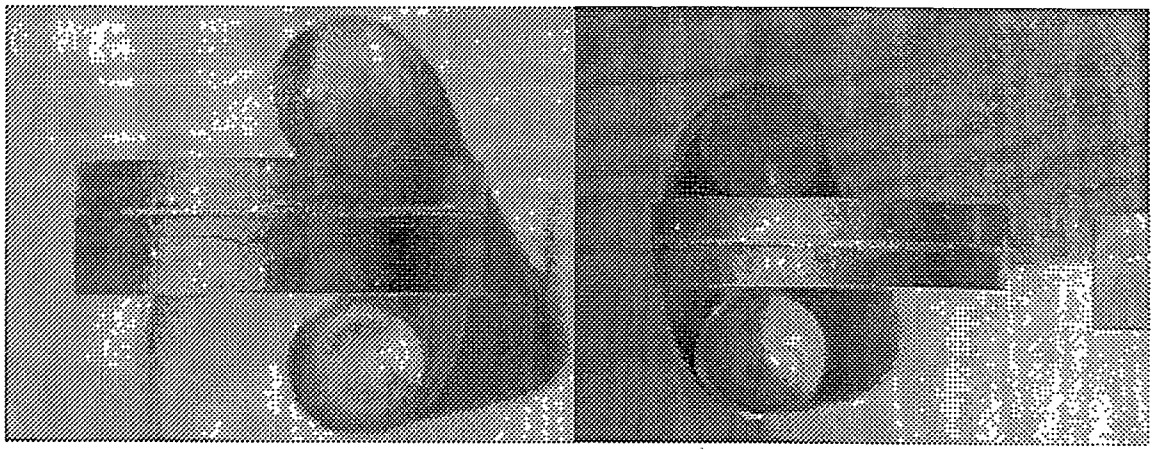

Figure 2 Ceramic membrane/ Haynes 230 joints. Left joint made at 10^{-9} atm. Right joint made at 10^{-5} atm.

- It has become evident that despite the relatively low chemical reactivity of these nickel-based brazing alloys, extensive reactions between the brazing alloy and the ceramic membrane occur when brazing. The following figure shows a typical braze/ceramic interface, with the corresponding chemical compositions obtained by EDS analysis.

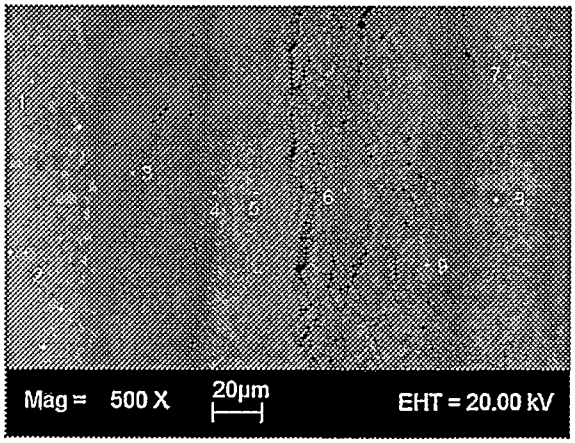

	1	2	3	4	5	6,9	7	8
Ni	56	21	70	0	0	0	0	0
Cr	25	30	9	0	0	0	0	0
W	13	40	0	0	0	0	0	0
Mo	1	0	0	0	0	0	0	0
Ti	0	0	0	0	0	0	0	0
Si	0	0	3	0	0	0	0	0
Fe	2	1	7	1	1	14	15	69
La	0	0	0	23	12	13	15	1
Sr	0	0	8?	1	15	8	8	2
O	0	0	0	76	71	65	62	29
Mn	4	4	0	0	0	0	0	0

Figure 3 Ceramic/braze interface. Compositions obtained using EDS.

The composition analyses of points 4 through 9 in Figure 3 show the extent of the reaction between the ceramic membrane and the brazing alloy. It can be observed that the first zone in contact with the brazing alloy has been depleted of both iron and strontium, while the next layer has only been iron-depleted. The formation of iron-rich "islands" can also be observed, which are not normally observed in the pre-brazing ceramic membrane.

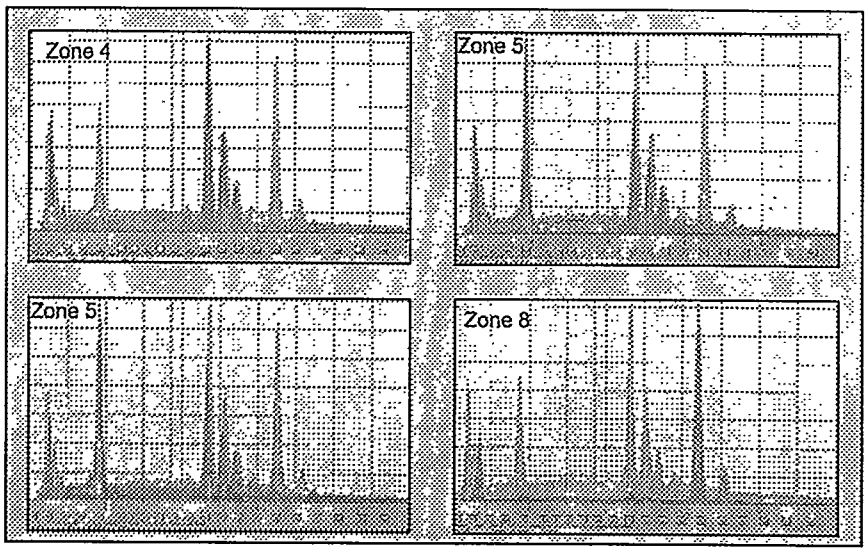

Figure 4 EDS spectra of different zones in previous figure.

The figure above compares the spectrum obtained from a "perovskite" sample before the brazing procedure takes place (green) with the spectrum observed after the braze has reacted with the ceramic surface (red). As can be seen, the composition of the ceramic close to the braze/membrane interface is significantly modified.

It is important to note that the reaction mechanism occurring at the interface has not been elucidated yet and that more research work on this system needs to be done. It is expected that changes in the chemistry of the brazing alloy can reduce the extent of the reaction between the braze and the ceramic.

It is suspected that the excessive reaction observed in the present experiments has a direct relationship with the cracks formed parallel to the ceramic/metal interface. Thus, by studying the reactions at the interface it would be possible to improve the integrity of the ceramic/metal joints.

In the future, a new series of experiments, in which both the chemical composition of the brazing alloy and the atmosphere under which the joining takes place are controlled, will be performed. If possible, samples will be prepared for mechanical shear test experiments.

Properties of the Joints

Testing techniques are being developed to measure and understand the mechanical properties of concentric metal-ceramic membrane joints. Since actual perovskite tubes are currently unavailable, we have chosen to study the properties of alumina tubes brazed around nickel-based alloy rods, using commercially available Ticusil™ brazing alloy. These materials were chosen

because the brazing of alumina with this alloy is well documented in the literature, and because Ni-based alloys with varying thermal expansions and elastic properties are available.

Table 1: Room Temperature Properties of Materials Used in Experiments

Material	CTE (μin/in/°C)	E (ksi)	0.2% YS (ksi)
Alumina	8.5	53,070	--
Invar	1	21,460	70.0
Hastelloy B2	10	31,038	57.5
Inconel 600	12	31,100	40.0

We are interested in how the properties of the base metal affect the residual stresses present in the brazed joint. This knowledge will help us design lower-stress joints for the ceramic membrane application.

The testing and analytical methods that are being developed will be applied to the La-Sr-Fe-O/Haynes 230 system when the ceramic (and associated property data) is available.

Measurement of Shear Strength

The geometry of the brazed rod-in-tube samples is shown schematically in Figure 5. The inner diameter of the ceramic tube is 0.257". Two different rod diameters are being used: 0.250" and 0.247". The rod and tube are each approximately 0.75" long, with a brazed overlap of approximately 0.30".

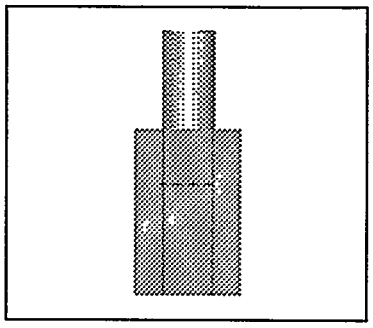

Figure 5 Mechanical tests specimens

The shear strength of the joints is measured by loading these samples in compression using an Instron testing machine. If the braze is weaker than the ceramic tube, the joint will fail by shearing the interface, however if the braze is stronger, the ceramic will fracture in compression.

Preliminary experiments run with Hastelloy B2 and Invar rods brazed to alumina, using a variety of metal rod diameters and cooling rates, led to the design of the current experiment. Brazed joints will be made from three different types of metal rods (Hastelloy B2, Invar, and Inconel 600), each in two diameters (0.250" and 0.247"). Different metals are being used to examine the impact of CTE mismatch on strength, while the different diameters will show if the filler metal thickness affects the strength of the brazed joint. Samples will be made under the following conditions, and their strength will be evaluated under compression loading:

1) Brazed at 850°C for 20min, and cooled at 1.7°/min
2) Brazed at 850°C for 20min, and cooled at 1.7°/min. Subjected to one thermal cycle between 100°C and 700°C, at a rate of 2°/min.
3) Brazed at 850°C for 20min, and cooled at 1.7°/min. Subjected to five thermal cycles between 100°C and 700°C, at a rate of 2°/min.

Some samples for condition 1 have already been made and tested. The following graph shows the experimental estimated shear strengths of the joints:

Table 2: Estimated Shear Strengths of Metal-Ceramic Joints

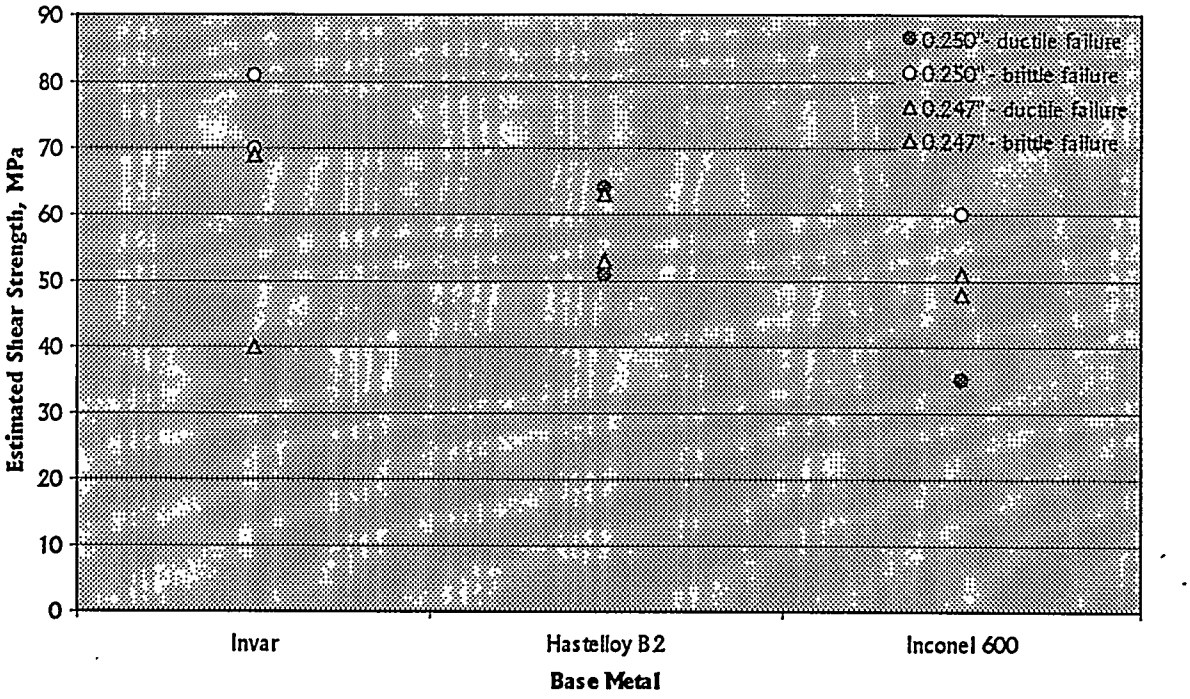

These few data points show some general trends about the character of metal-ceramic joints. As the CTE mismatch between the metal and ceramic increase, the strength of the resultant joint decreases. Also, for this geometry, a negative CTE mismatch (ceramic expands more than metal, i.e. the Invar/Alumina joint) does not seem to be as detrimental as a positive mismatch. The filler metal thickness only seems to affect the strength of the Invar/Alumina joint.

Two distinct fracture modes were observed in these samples: brittle failure in the ceramic and ductile failure in the braze. We hope to correlate the CTE mismatch and filler metal thickness of the joint to the failure mode once more data is available.

Finite Element Modeling

Finite element models for metal-ceramic joints are being made using the ABAQUS software package. Residual stresses develop in these joints during cooling. The system can be considered to be stress-free at the solidus temperature of the braze alloy (780°C for Ticusil™). However, as the joint cools, one member often contracts more than the other, which can result in complicated residual stresses when the joint is at room temperature. The metal usually contracts more than the ceramic, since the CTE of the metal is usually larger than that of the ceramic.

The newest model has the same geometry as the samples used for mechanical testing. It models the stresses developed upon cooling from 780°C to 20°C, and temperature-dependant materials

properties are taken into consideration. It is assumed that both the alumina and base metal are perfectly elastic, and the Ticusil™ layer is perfectly plastic. The finite elements are 8-node axisymmetric elements with reduced integration, and the nodes lying on the Z-axis are constrained in the radial direction.

The magnitude of CTE mismatch between the ceramic and metal greatly influences the residual stresses that are present after cooling. The following figures depict the axial stresses that are present after brazing. The contour map on the right is of a Hastelloy B2 / Ticusil™ / alumina joint (the metal is on the upper right, ceramic on lower left). The metal along the interface is stressed in tension, because it wants to contract but is constrained by the ceramic. The Ticusil™ bonding the components has plastically deformed to accommodate the different contractions of the metal and ceramic.

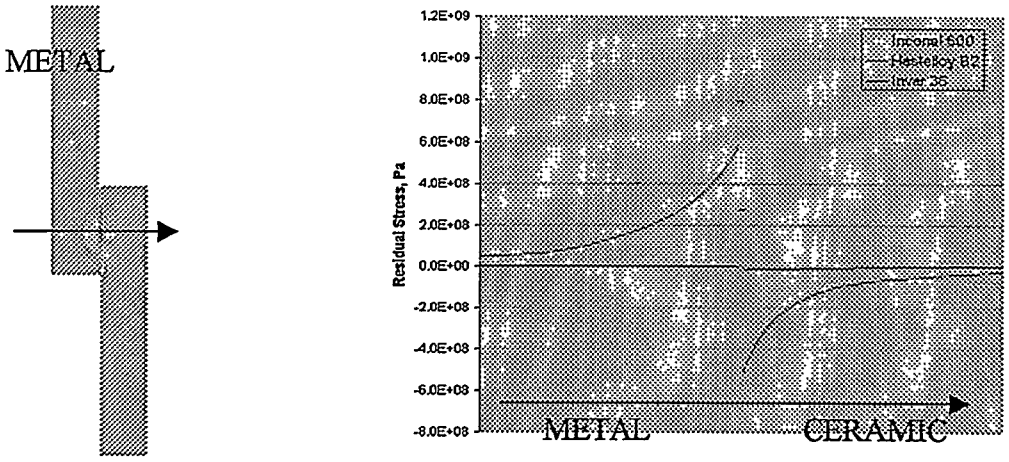

Figure 6: (L) Contour map of residual axial stresses in a Hastelloy B2 / Ticusil™ / Alumina joint.

(R) Residual axial stresses along themidpoint of the braze.

The graph to the left of the contour map compares the axial stresses present across the midsection of a brazed joint for the three different base metals. It is clear that the joints in which the CTE of the metal is much greater than that of the ceramic (Hastelloy B2 and Inconel 600) have much larger residual stresses present than joints where the CTE of the metal is smaller than that of the ceramic (Invar 36).

It follows that joints that have small residual stresses will be stronger than those that have large residual stresses, and this prediction agrees with early experimental results.

Future Work:

Using the results obtained from the experimental work, new joining techniques will be designed and tested. Different brazing alloys will be put to test. A complete analysis of the interfaces created will be performed. The mechanical tests will continue, and the strength and thermal fatigue properties of joints will be characterized. From the experiments and numerical analysis on concentric ceramic/metal joints, design rules will be developed.

Conclusions:

Preliminary La-Sr-Fe-O/Haynes 230 joints have been made using amorphous nickel-based filler metals. The fact that these conventional alloys are capable of wetting the ceramic is a positive and a somewhat surprising outcome, although further analysis is required to understand better the phenomena taking place at the ceramic/metal interface.
It has been found that there is a large chemical interaction between the ceramic surface and the braze. This reactivity appears to be affected by the actual oxygen partial pressure under which the joining process takes place, although this has yet to be confirmed. There is also evidence that the extent of the interfacial reactions between the brazing alloy and the ceramic might influence the integrity of the ceramic/metal joint created. An experimental setup for measuring the mechanical properties of concentric ceramic/metal joints has been built and operated. Finite element models of concentric ceramic/metal joints have been made. It is expected that the same experimental program can be performed on the ceramic membrane once the first perovskite tubes are fabricated and sent to us.

TASK 3: Determine material mechanical properties under conditions of high temperature and reactive atmosphere

Prof. Sukumar Bandopadhyay & Dr. Nagendra Nagabhushana
University of Alaska Fairbanks

ABSTRACT

In the fourth quarter, first experiments on the mechanical strength of La-Sr-Fe-O ceramic tubes are reported. Tubes of Cr_2O_3 doped $LaSrFeO_3$ (20576-25 Px and 20576-25t) were supplied by BP for strength characterization. The tubes were tested at room temperature in C-Ring geometry according to ASTM C1323. The results indicate that tubes 20576-25t exhibited higher fracture as compared to 20576-25Px. A distinctive change in fracture morphology was also observed.

Experimental Set up:

The Perovskite oxide tubes 20576-25 Px and 20576-25t were cut in to C-Ring specimens. The cut surfaces were polished and the edges beveled. The room temperature experimental set up are as show in figure 1 a and b. The C-ring specimens are placed between two hardened platens and a thin strip of compliant paper inserted to reduce friction and to align the specimens. The tubes were loaded monotonically to fracture and the maximum load recorded to calculate the fracture Stress. The fracture surfaces were examined to characterize the fracture characteristics.

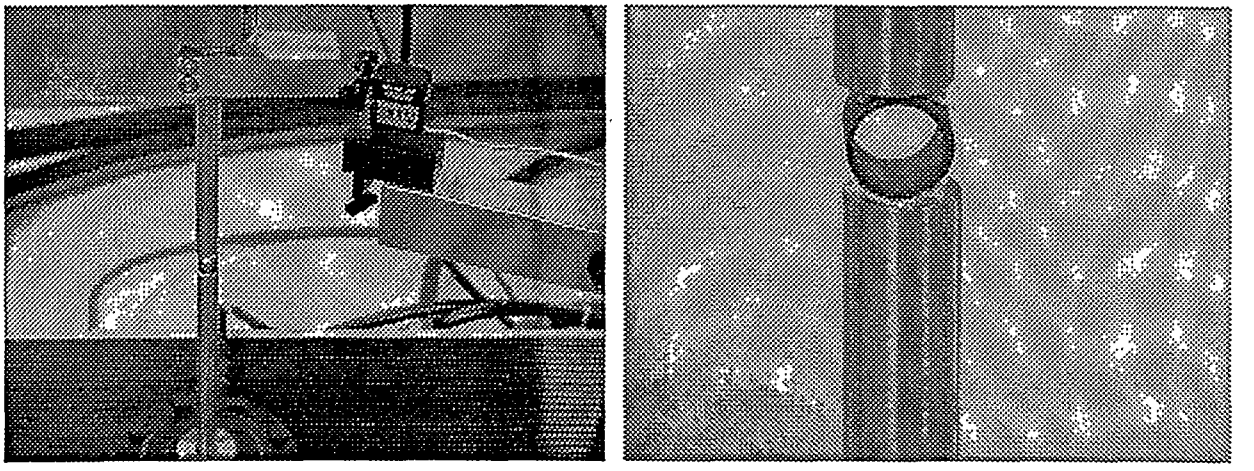

(a) (b)

Fig.1 Experimental set up for characterizing fracture strength in C-ring specimen geometry.

OBSERVATIONS

The tubes 20576 were cut into C-rings for mechanical strength characterization. C-ring specimen loaded in diametral compression leads to a maximum tensile stress at the outer surface. The strength distribution and flaw population of the tubes can thus be evaluated on the outer surface of the tube.

The tubes provided were not uniform through out the length and C-ring specimens showed a variation in the wall thickness. As shown in the figure below, C-rings from 20576-25 Px were uniform in the outer diameter, but showed a large variation in the wall thickness. On the other hand, 20576-25t showed fewer scatters in the wall thickness but was not uniform in the outer diameter. These variations were expected to be reflecting in the strength distribution and thus the strength values were calculated for every specimen as a standard procedure.

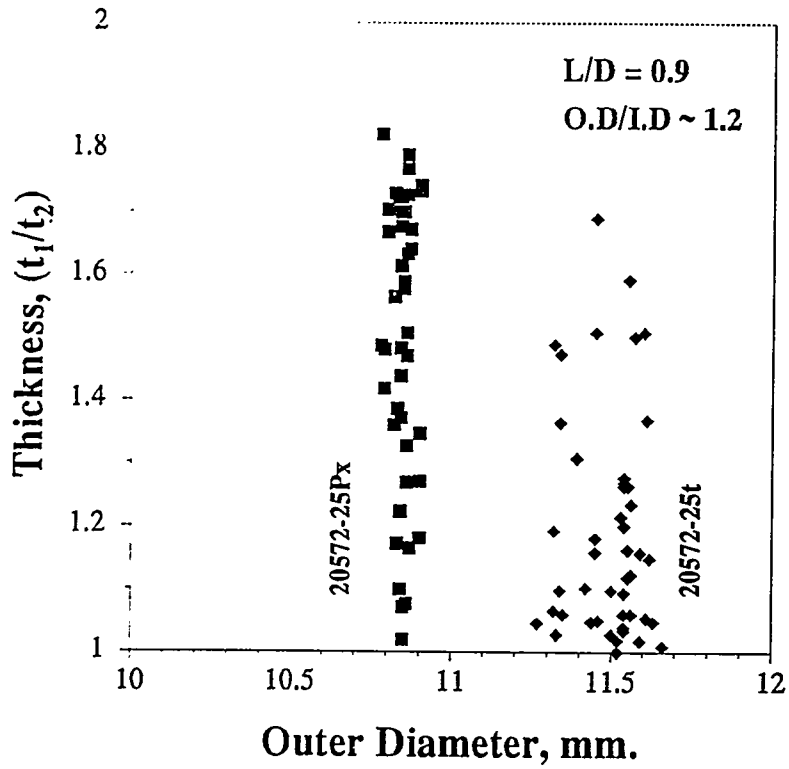

Fig 2. Variation in the C- ring specimen dimensions

Strength of 20576 tubes:

The maximum fracture strength of the C-Ring specimens were calculated from the equation:

$$\sigma_{\theta\max} = \frac{PR}{btr_o}\left[\frac{r_o - r_a}{r_a - R}\right]$$

Where r_o - is the outer radius of the C-Ring, b – the width of the ring, t – thickness and P the fracture load. However, the actual fracture strength is calculated from the measure angle of fracture from the mid plane.

The measured strength of the 20576 tubes are as shown in table 1. The maximum strength of 429 MPa observed in 20576-25t was twice of that observed in 20576-25Px (210 MPa). However, the standard deviation in the strength values of 20576-25t was also higher than that observed in 20576-25Px. This could possibly be attributed to the variation observed in the specimen geometry.

Table1: Strength of 20576 tubes.

	20576-25 Px	20576- 25 t
Minimum, MPa	114.47	175.53
Maximum, MPa	210.43	429.18
Sum	1839.5628	3693.52
Points	11	12
Mean, MPa	167.23	307.79
Median, MPa	188.47	302.05
RMS, MPa	170.64	318.85
Std Deviation	35.62	86.95
Variance	1269.19	7561.61

Fracture Observations:

Macroscopic:

Macroscopic observation indicated a distinctive difference in fracture morphology of 20576-25Px and 20576-25t. In 25 Px, fractures in all the specimens tested were fractured at midplane. The fracture surfaces were smooth and seemingly dominated by surface flaws. On the other hand, specimens of 25t shattered during testing and very often the fracture plane was at an angle from the midplane. The fracture morphology was predominantly jagged with interspersing planes of smooth fracture.

Based on the macroscopic fracture observation, a simple two-parameter Weibull plot was generated to characterize the strength and the observed variation in wall thickness of individual

C-rings. A complete Weibull plot is to be generated from microscopic observation of fracture and the observed angle of fracture.

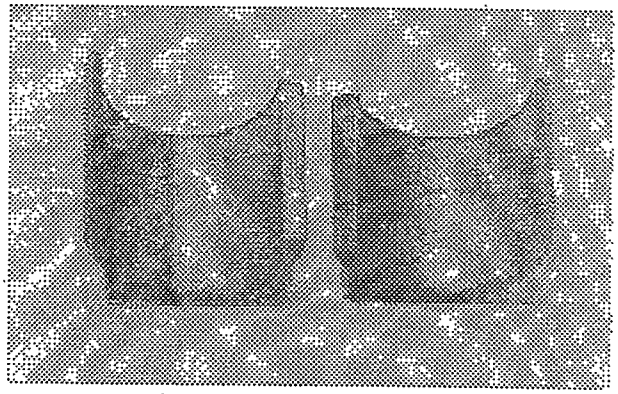

a) 25 Px : Surface and Volume flaw

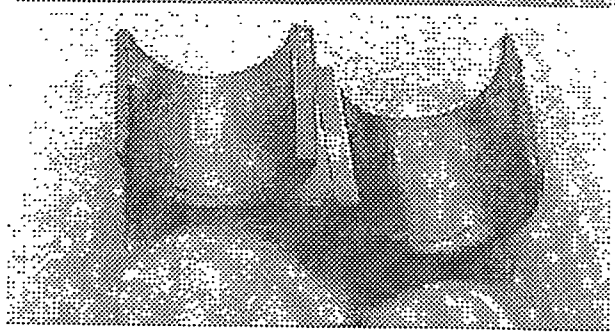

b) 25 Px : Surface flaw

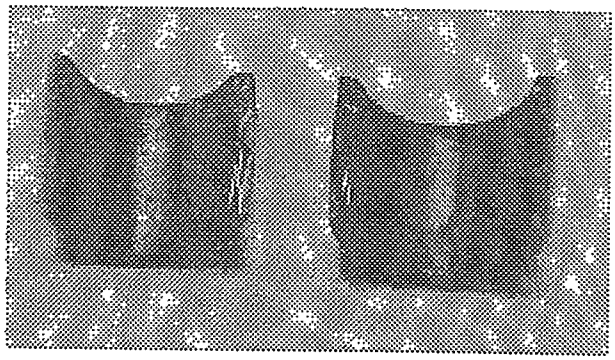

c) 25t : Jagged fracture and surface flaw dominated

Fig 3 Macroscopic fracture observed in 20576 tubes. a & b – Fracture dominated by surface and volume flaws in 25Px. The fracture is smooth and planar. c) Fracture in 25t is jagged and dominated by surface flaws.

A detailed fractographic study is planned to characterize the active fracture mechanism and the influence of preexisting flaws on the strength and fracture characteristics.

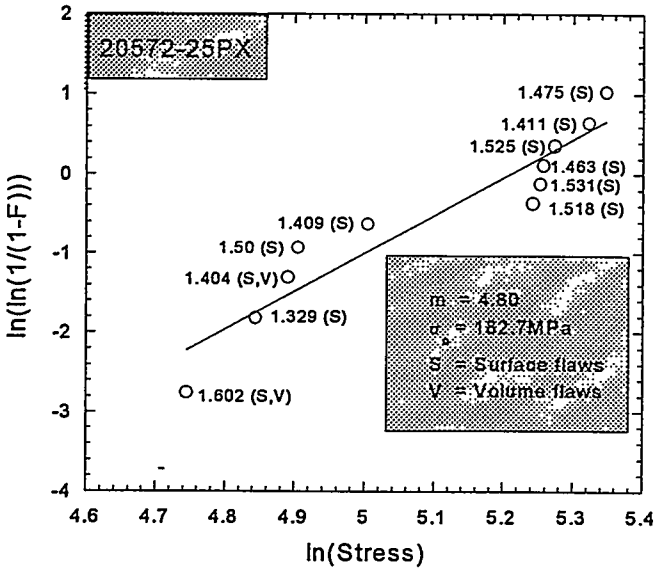

a) 20576-25Px

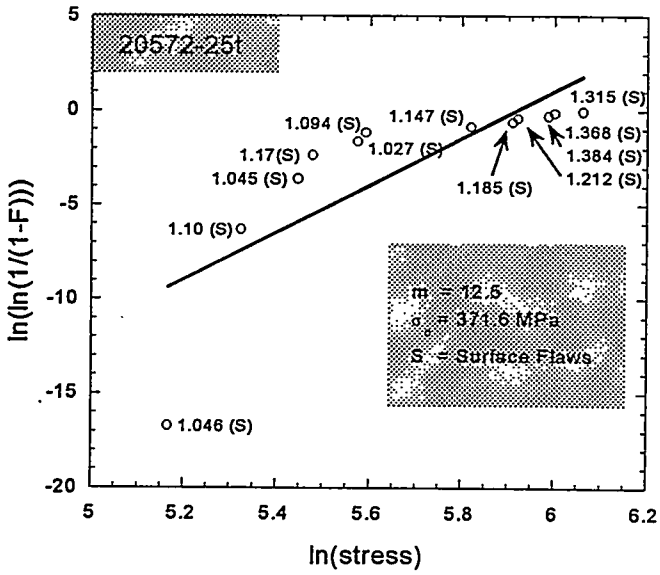

b) 20576-25t

Fig.4 Weibull plot of unadjusted strength distributions for all specimens tested at room temperature. The sample dimensions (t_1/t_2) and observed macroscopic fracture are overlaid on the plot.

The Weibull plot indicated an increased Weibull modulus (m) in the 25t samples as compared to 25Px specimens. The characteristic fracture stress σ_o, was also higher in 25t samples at 372 MPa as compared to 183 MPa for 25 Px samples.

Task 4: Preparation and characterization of Dense Ceramic Oxygen Permeable Membrane

Dr. Harlan U. Anderson, Director of EMARC
Dr. Wayne Huebner, Dr. Yixiang Xie
University of Missouri- Rolla

Summary

In this quarter, a modified Pechini liquid mixing method [1, 2] was used to produce mixed-cationic oxide powders of compositions, $La_{0.19}Sr_{0.80}Fe_{0.90}Cr_{0.10}O_{3-\delta}$, $La_{0.19}Sr_{0.80}Fe_{0.80}Cr_{0.20}O_{3-\delta}$, $La_{0.19}Sr_{0.80}Fe_{0.65}Cr_{0.35}O_{3-\delta}$, $La_{0.59}Sr_{0.40}Fe_{0.85}Ti_{0.15}O_{3-\delta}$, $La_{0.59}Sr_{0.40}Fe_{0.85}Cr_{0.15}O_{3-\delta}$, $(La_{0.60}Sr_{0.40})_{0.99}FeO_{3-\delta}$, $La_{0.19}Sr_{0.80}Fe_{0.70}Cr_{0.20}Ti_{0.10}Mg_{0.01}O_{3-\delta}$, $La_{0.19}Sr_{0.80}Fe_{0.70}Cr_{0.20}Nb_{0.10}Mg_{0.01}O_{3-\delta}$, $La_{0.20}Sr_{0.80}Fe_{0.70}Cr_{0.20}Ti_{0.10}O_{3-\delta}$, and $La_{0.20}Sr_{0.80}Fe_{0.70}Cr_{0.20}Nb_{0.10}O_{3-\delta}$, for phase study. Sintering process and x-ray diffraction study indicate 1) Cr doping should be restricted to a certain level, 2) a thermodynamic reversible process is recommended to avoid phase separation (decomposition), 3. A higher Sr doping should also combine with a Cr doping, 4) $(La_{0.60}Sr_{0.40})_{0.99}FeO_{3-\delta}$ single phase can be reached by a reversible sintering process After applying a stress on disk, XRD shows an orientation change. Sintered disks were sent to the MIT mechanical and sealing research group on their request.

Introduction

Dense ceramic membrane materials have been studied by a team with NIST through Praxair and British Petroleum Chemical for use as oxygen separation membranes for gas production and syngas application. Leading dense ceramic membrane materials for high temperature oxygen separation have been identified, which are oxide perovskites with a general formula ABO_3 with La, Sr at the A site and the B site primarily occupied by Fe. Due to the significant progress of the NIST program, a new team has been formed for further investigation on these materials through this UAF/DOE program.

As a part of the team, this group agreed to study the processes of making compositions, pressing, and sintering and to provide sintered disks using powders with selected compositions from $La_xSr_{1-x}FeO_{3-\delta}$ which is doped with either Ti, Cr, Ga, or Zr to other team members. Meanwhile this group engaged in characterization of the selected compositions through XRD, electrical conductivity, thermoelectric power measurements, TGA, and thermal expansion as the first phase task of the program. In our previous quarterly, semiannual, and annual reports through our XRD, TGA and thermal expansion study we have concluded that these oxides keep their major perovskite structure and are reversible at a temperature lower than 1000 °C in a strong reducing atmosphere up to 90% CO with a balance gas, CO_2 ($logPO_2$, -16.1). However, they lose phase stability in stronger reducing atmospheres, which is further confirmed by TGA and thermal expansion data. We also concluded that 1) instability of perovskite by A site Sr doping can be compensated by Fe multi-valence states. 2) B site Ti and Cr doping enhance the stability. Our previous research on non-ferrite lanthanum-strontium perovskite with Zr dopant indicates that Zr does not help phase stability possibly due to its larger radius than that of major B site element. We do not recommend Zr as a B site dopant. While these perovskites are not be able to maintain

a single phase under the wide application conditions, a composition of XRD single phase perovskite prepared under air atmosphere is absolutely necessary to establish a basis for a further intense study. Therefore, in this quarter, we have focused on the single phase composition study. Previous study on the high Sr doping composition, $La_{0.19}Sr_{0.80}FeO_{3-\delta}$, indicates that strontium oxide, SrO second phase is easy to be formed in the major perovskite matrix and reversibility is unlikely. To increase the perovskite single phase stability, either lower the Sr doping at A site or dope Cr at B site at an appropriate level.

Experimental

1. Powder Preparation

A modified Pechini liquid mixing method [1, 2] was used to produce powders.

a) Chemicals

Vendor	Catalog No.	Name	Purity
Alfa Aesar	36665	Citric Acid, Monohydrate	99.0-102.0%
Fisher Scientific	E178-4	Ethylene Glycol	$H_2O < 0.02\%$
Fisher Scientific	A509SK-212	Nitric Acid	total metals < 0.1ppm
Alfa Aesar	16639	Lanthanum Carbonate	99.9%
Alfa Aesar	14343	Strontium Carbonate	99%
Alfa Aesar	33315	Iron (III) Nitrate	98.0-101.0%
		Niobium Oxalate	
Aldrich	32,525-2	Titanium diisopropoxide bis(acetyl-acetonate)	
Alfa Aesar	11565	Chromium (III) Nitrate	98.5%

All metal compounds were quantified every two weeks and kept in tape sealed containers. For preparation of per 30 gram powder, the water, Citric Acid, and Ethylene Glycol content was 200 ml, 50 grams, and 20 grams respectively.

b) Processing

(1) Citric Acid Monohydrate, and Ethylene Glycol are added into distilled water with magnetic stirring in a beaker.
(2) Carbonate(s) is(are) added into the solution.
(3) Slowly nitric acid was added into the liquid mixture until the liquid became transparent.
(4) Dissolve nitrate(s) into the transparent liquid.
(5) Filter the transparent liquid to eliminate dark solid insoluble residue.
(6) Stir the liquid overnight.
(7) Carefully evaporate water from the liquid on a hot plate until it solidifies.
(8) Put the beaker into an oven at a temperature at about 150 EC for 48 hours.

(9) Transfer the resulted mixture into crucibles then put the crucibles into a furnace.
(10) Increase furnace temperature to 300 EC for over a 12 hours period and hold that temperature for 12 hours.
(11) Increase temperature to 800 °C and hold the temperature for 6 hours before cooling.
(12) Powder may be heated at 1250 °C for XRD purpose. The temperature of powder treatment is labeled with the XRD pattern.

2. Sintering Process

a) Powder Treatment

step	Rate, °C/minute	Temperature, °C	Dwelling, hour
1	5	1250	6
2	Natural cooling	25	

b) New Sintering Process of $(La_{0.60}Sr_{0.40})_{0.99}FeO_{3-\delta}$

step	Rate, °C/minute	Temperature, °C	Dwelling
1	0 2	100	2
2	0 2	200	2
3	0 2	300	3
4	0 2	400	5
5	0 5	800	2
6	0.5	1200	6
7	-0.5	700	3
8	-0.5	25	

3. Powder X-ray diffraction measurements were carried on a SINTAG 2000 x-ray diffractometer operating with Cu Kα1 radiation. A stepped scan using a step size of 0.03° was employed.

Results and Discussion

X-Ray Diffraction

Previously we concluded that 800 °C might not be sufficient to obtain a single perovskite phase. Specifically Cr doped compositions have a chromate second phase in the powders calcined at 800 °C, which disappears at about 1200 °C. Both Cr and Ti doping help stabilization of the doped perovskite structure for the compositions of interest. However, it is evident that the stability of $SrCrO_4$ creates problems with obtaining single phase perovskite. Figure 1 shows XRD patterns corresponding to the powders of $La_{0.19}Sr_{0.80}Fe_{0.90}Cr_{0.10}O_{3-\delta}$, $La_{0.19}Sr_{0.80}Fe_{0.80}Cr_{0.20}O_{3-\delta}$, $La_{0.19}Sr_{0.80}Fe_{0.65}Cr_{0.35}O_{3-\delta}$, treated at 1250 °C and furnace cooled. The 35% Cr doping composition has a significant $SrCrO_4$ second phase, which clearly demonstrates the problem with higher Cr doping. Figure 2 shows XRD patterns corresponding to the powders of

$La_{0.59}Sr_{0.40}Fe_{0.85}Ti_{0.15}O_{3-\delta}$, $La_{0.59}Sr_{0.40}Fe_{0.85}Cr_{0.15}O_{3-\delta}$, treated at 1250°C with furnace cooling. While the intensity scale-up indicates some second and/or third phase(s) in these compositions, it appears to be possible to obtain XRD single-phase structures for these compositions. TGA study has shown that perovskite oxides lose oxygen at a higher temperature. Under an atmosphere of lower oxygen partial pressure, they lose even more oxygen, which could be the reason of the second phase formation. A furnace cooling process is far from thermodynamic equilibrium. So a slower cooling process may be required to obtain single-phase perovskite.

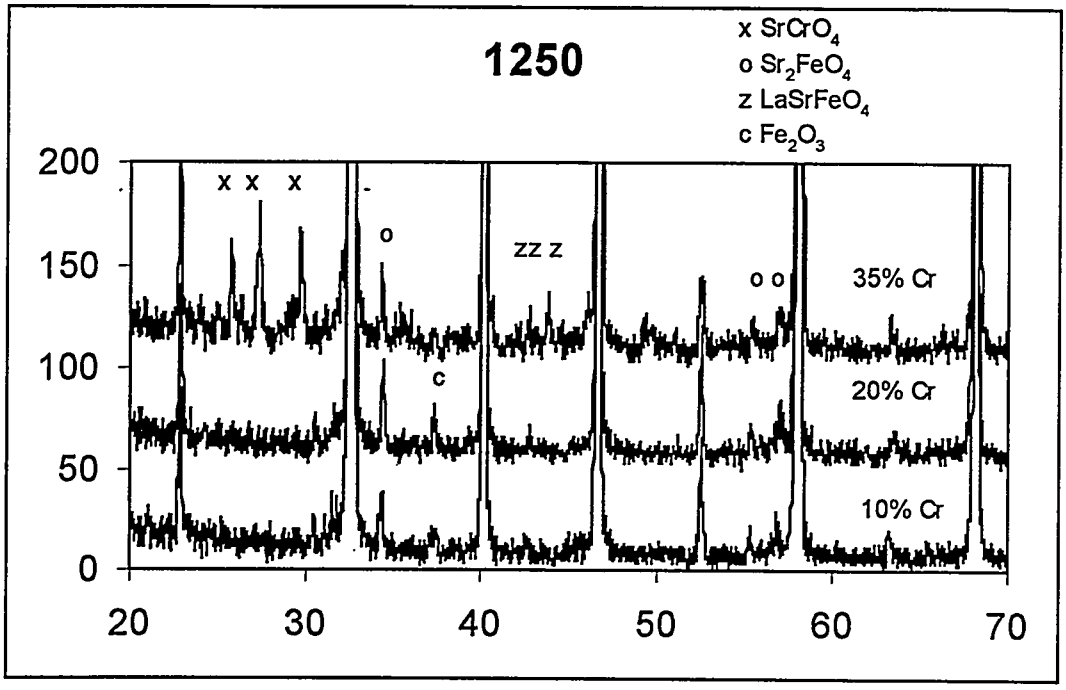

Figure 1. Powder X-Ray Diffraction Patterns taken from 1250 °C heat treatment powders of $La_{0.19}Sr_{0.80}Fe_{0.90}Cr_{0.10}O_{3-\delta}$, $La_{0.19}Sr_{0.80}Fe_{0.80}Cr_{0.20}O_{3-\delta}$, $La_{0.19}Sr_{0.80}Fe_{0.65}Cr_{0.35}O_{3-\delta}$

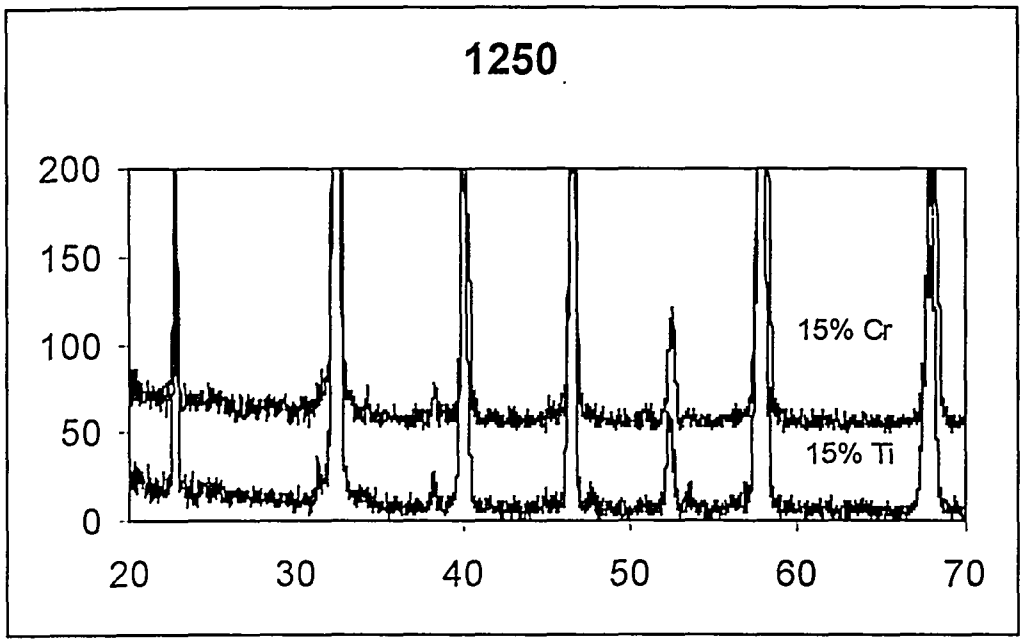

Figure 2. Powder X-Ray Diffraction Patterns taken from 1250 °C heat treatment powders of $La_{0.59}Sr_{0.40}Fe_{0.85}Ti_{0.15}O_{3-\delta}$, $La_{0.59}Sr_{0.40}Fe_{0.85}Cr_{0.15}O_{3-\delta}$

Figure 3 shows the XRD patterns of $(La_{0.60}Sr_{0.40})_{0.99}FeO_{3-\delta}$, taken from samples prepared through different processes. The lower two patterns are corresponding to powders treated under air with furnace cooling step. While we can see the evidence of $LaSrFeO_4$ and/or Fe_2O_3 phase(s) in the two patterns, the third pattern of disk sample cooled under nitrogen shows much stronger second and third phases. The top pattern is corresponding to the disk sintered in air by the new slow process, specifically a very slow cooling procedure. This pattern shows no evidence of second phase. All of this clearly suggest that we can process this composition to a dense single phase structure, $(La_{0.60}Sr_{0.40})_{0.99}FeO_{3-\delta}$. Figure 4 is the normal XRD pattern of the disk with the composition $(La_{0.60}Sr_{0.40})_{0.99}FeO_{3-\delta}$ and prepared through the new sintering process.

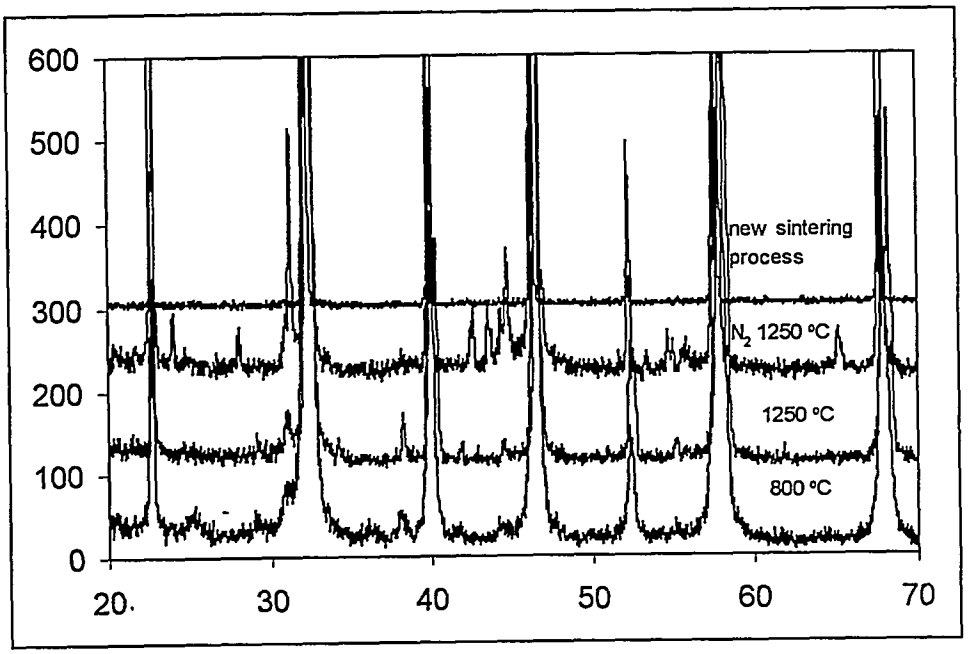

Figure 3. XRD patterns of $(La_{0.60}Sr_{0.40})_{0.99}FeO_{3-\delta}$

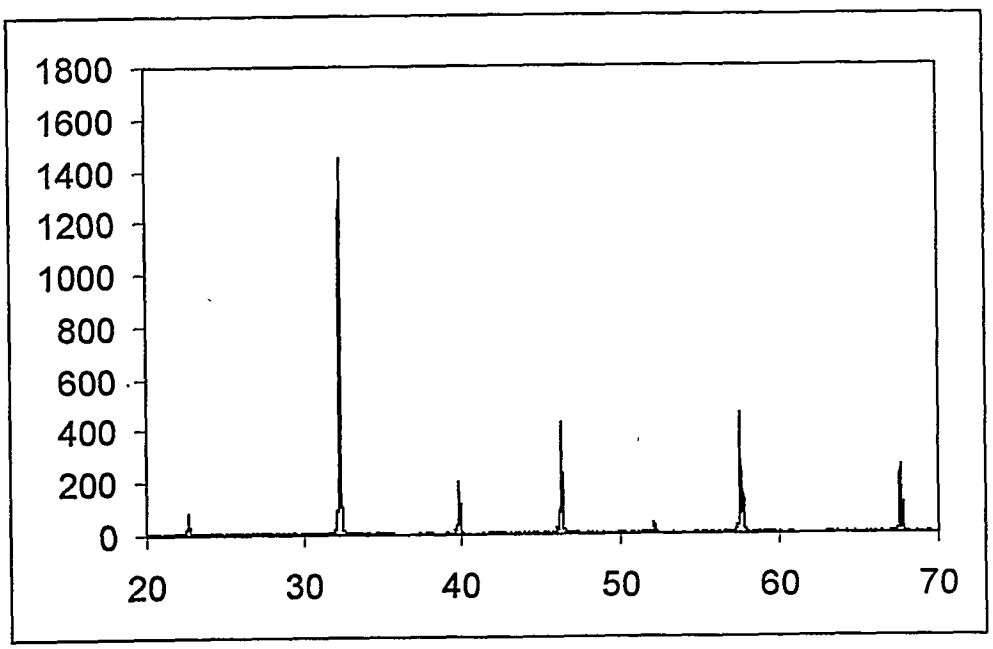

Figure 4. XRD pattern of disk $(La_{0.60}Sr_{0.40})_{0.99}FeO_{3-\delta}$ by new process

Stress Analysis

A study on rhombohedral perovskite oxides indicates that applying a stress on a sintered bulk material will result in an orientation change. We applied a stress, 1000 psi for 5 hours on a sintered disk that was prepared by the new sintering process. Figure 5 is the patterns of the disk taken before and after applying the stress. After applying the stress on the disk the splitting peaks intensity ration changed which may reflect the orientation change and the peak shift may reflect a change of angles, lattice parameters. The after stress XRD pattern was taken after the stress was released at least 20 hours, therefore, the lattice parameter change (if any) may be reflected in a stress-strain curve as a part of plastic (ductile) deformation. Figure 6 is a plot of stress-strain, forward-reverse circulation on a sintered disk of $(La_{0.60}Sr_{0.40})_{0.99}FeO_{3-\delta}$. Each circle has a plastic deformation (move toward to right). The circles of middle range have larger movement. Figure 7 is a plot of a single cycle stress-strain measurement.

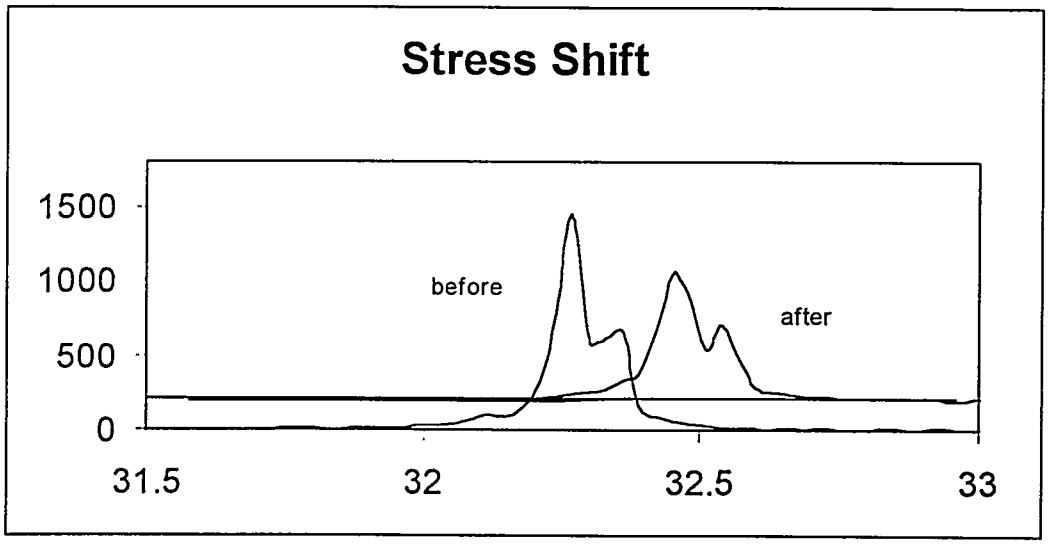

Figure 5. XRD patterns of disk $(La_{0.60}Sr_{0.40})_{0.99}FeO_{3-\delta}$ before and after stress

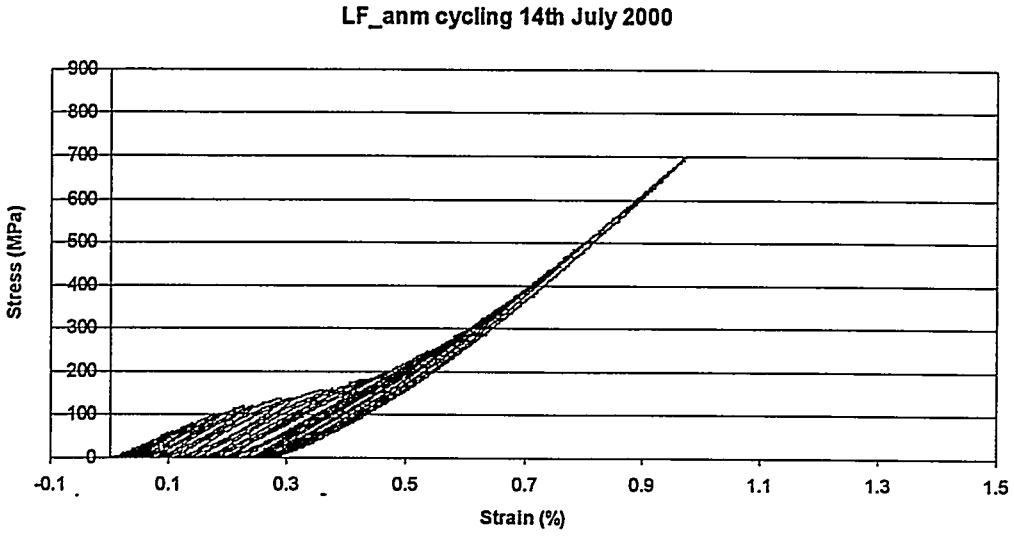

Figure 6. Stress-strain circulation on disk of $(La_{0.60}Sr_{0.40})_{0.99}FeO_{3-\delta}$

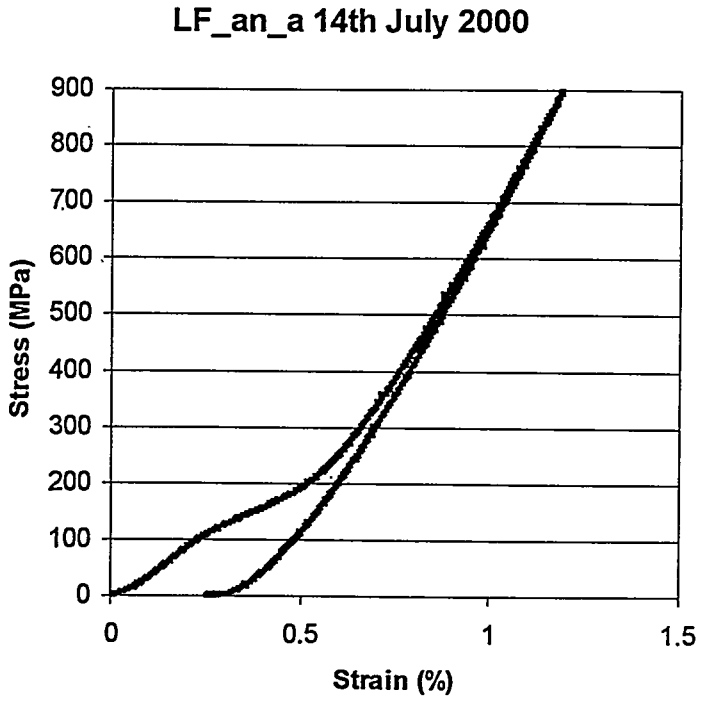

Figure 7. Single forward-reverse stress-strain cycle on disk of $(La_{0.60}Sr_{0.40})_{0.99}FeO_{3-\delta}$

Conclusion

1) Disks made using $(La_{0.60}Sr_{0.40})_{0.99}FeO_{3-\delta}$ sintered in air and cooled in nitrogen do not crack during processing, however, these specimens are not single phase stucture.

2) Disks made using $(La_{0.60}Sr_{0.40})_{0.99}FeO_{3-\delta}$ sintered in air and "slowly" cooled in air are single phase perovskite, however cracking occurs.

3) The addition of either Ti or Cr (5-15%) into the B site of $(La_{0.60}Sr_{0.40})_{0.99}FeO_{3-\delta}$ tends to allow the formation of single phase perovskite structure. We still are not sure if crack free specimens can be produced in an air atmosphere.

Program for next quarter

1) BP Chemical will complete fabrication of porous $(La_{0.60}Sr_{0.40})_{0.99}FeO_{3-\delta}$ tubes from PSC powder.
2) Provide PSC powder to MIT as required.

3) Provide sintered PSC disks to larson's group at MIT as necessary.

4) Provide sintered PSC disks to University of Houston as necessary.

5) Provide sintered PSC disks to UIC.

6) Initiate studies on Ga perovskite compositions (task 4.2.1.1, and task 4.2.1.2).

References

1. M. P. Pechini, "Method of Preparing Lead and Alkaline Earth Titanates and Niobates and Coating Method Using the Same to Form a Capacitor," U. S. Pat. No. 3,330,697, 1967.

2. N. G. Eror and H. U. Anderson, 'Polymeric Precursor Synthesis of Ceramic Materials"; pp571-77 in Better Ceramics through Chemistry II, Proceedings of Materials Research Society Symposium, Palo Alto, CA, April 1986. Edited by C. J. Brinker, D. E. Clark, and D. R. Ulrich. Materials Research Society, Pittsburgh, PA, 1986.

TASK 5: Assessment of Microstructure of the Membrane Materials to Evaluate the Effects of vacancy-Impurity Association, defect Clusters, and Vacancy Dopant Association on the Membrane Performance and Stability

Professor Niegel Brown
University of Illinois, Chicago Circle

Analysis of samples 1 and 2 by scanning transmission electron microscopy is now complete. Differences in microstructures are observed for the samples prepared under different conditions and with different compositions. Work is continuing to analyze the data and compare with the transport measurements to infer the effect of microstructure on the properties.

Task 6: Measurement of Surface Activation/Reaction rates in Ion Transport Membranes using Isotope Tracer and Transient Kinetic Techniques.

Prof. Alan Jacobson, University of Houston/University of Toronto

Progress during past 3 months at the University of Toronto

(1) Oxygen isotope infusion under gradientless conditions.

As planned, the initial set of oxygen infusions were carried out during the current quarter, and the resulting profiles analyzed to extract values of k_O and D_O, the surface exchange coefficient and bulk diffusion coefficient respectively, for oxygen in two ferrite materials. The following table summarizes the materials, the conditions for the infusions and the derived transport parameters.

Materials Studied	**T(C)**	**Oxygen activity** (* assume WGS eq.)	**D_O / cm^2 s^{-1}**	**k_O / cm s^{-1}** (* not redox)
$La_{0.2}Sr_{0.8}FeO_{3-x}$	850	0.2	5.6×10^{-7}	9×10^{-6}
$La_{0.2}Sr_{0.8}FeO_{3-x}$	750	0.2	1.3×10^{-7}	4.8×10^{-6}
$La_{0.2}Sr_{0.8}FeO_{3-x}$	850	10^{-16} *	$<9 \times 10^{-7}$	$>8 \times 10^{-6}$ *
$La_{0.2}Sr_{0.8}Fe_{0.8}Cr_{0.2}O_{3-x}$	850	0.2	9×10^{-7}	4×10^{-5}
$La_{0.2}Sr_{0.8}Fe_{0.8}Cr_{0.2}O_{3-x}$	750	0.2	2.1×10^{-7}	1.6×10^{-5}
$La_{0.2}Sr_{0.8}Fe_{0.8}Cr_{0.2}O_{3-x}$	750	10^{-17} *	N/A	N/A

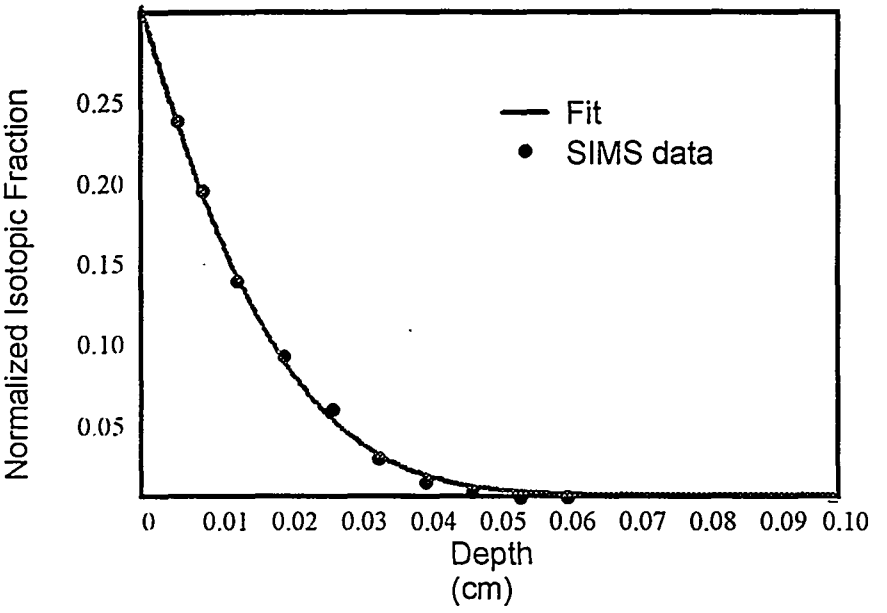

Fig 1 A typical 18O profile and the fit to the data giving D_O and k_O

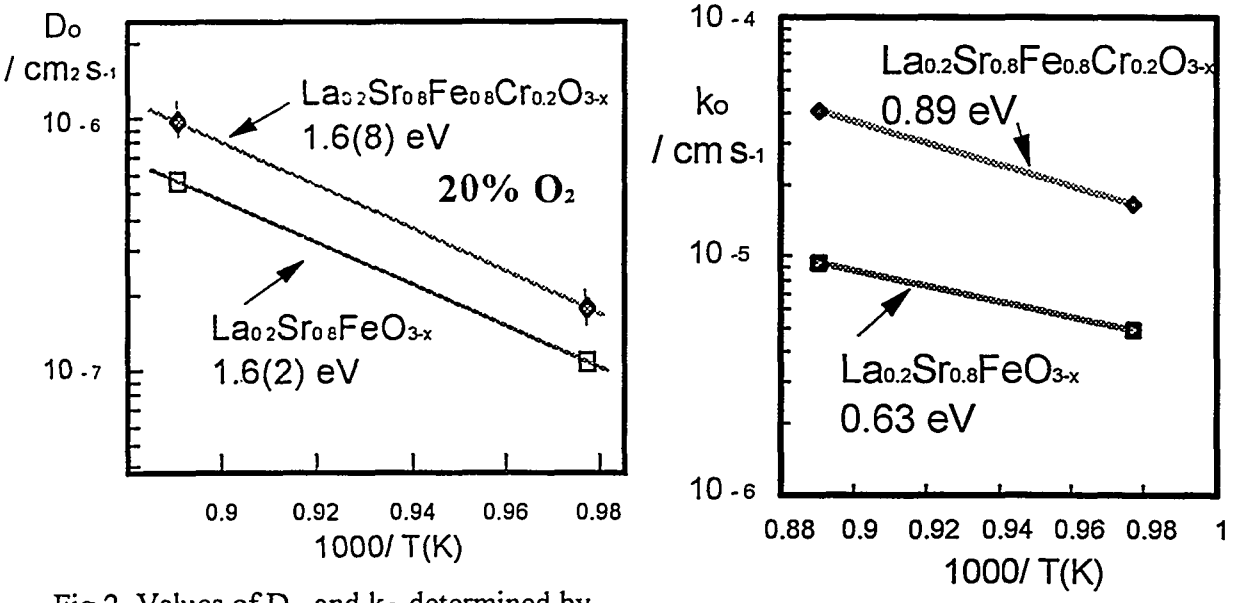

Fig.2. Values of D_O and k_O determined by

SIMS analysis 18O isotope profiles

The $La_{0.2}Sr_{0.8}FeO_{3-x}$ material was prepared by the U. Missouri group and the $La_{0.2}Sr_{0.8}Fe_{0.8}Cr_{0.2}O_{3-x}$ material from Praxair Specialty Ceramics. Infusions in 20% oxygen atmosphere were performed at the two temperatures for both materials. One of the resulting ^{18}O profiles is shown in Figure 1. Also shown in the Figure is the simulated profile generated using the derived values of k_O and D_O. These values were derived from the simple 1-D diffusion equation solution assuming constant gas phase isotopic composition. This condition was

essentially true for the oxygen atmospheres, but not for the reducing atmospheres (see below) Figures 2 and 3 show Arrhenius plots of the derived values of k_O and D_O, for these materials infused in air. In order to compare these values to those obtained in conductivity relaxation experiments, and to calculate the vacancy diffusion coefficient, D_V, from the derived values of D_O, requires currently unavailable information about the vacancy concentrations at the infusion conditions is required. With reasonable assumptions about the vacancy concentrations, the values above agree with the conductivity relaxation results obtained at the University of Houston. Preliminary infusions were also made in atmospheres characteristic of the fuel side of a methane partial oxidation membrane. In these cases, the gas atmosphere was $C^{18}O_2$:H_2:Ar (proportions 5:5:90). Unless equilibrium in the water-gas-shift (WGS) reaction is established, the oxygen potential is undefined for this mixture and the oxidation state of the material is controlled by the dynamic balance between reduction by hydrogen (and some CO) and oxidation by CO_2 (and some H_2O). The conversion in the reverse WGS reaction was monitored during the experiment and did not reach equilibrium. At the 1 Aug meeting, the WGS equilibrium was erroneously reported to be achieved, but in fact only 10% conversion of the CO_2:H_2 mixture to equilibrium was achieved in the 750°C experiment. Further complications arise from the extremely rapid surface exchange of CO_2 with the surface. This has been reported for other oxides. Rapid exchange is advantageous in that it assures that sufficient oxygen is infused for proper measurement of the diffusion coefficient. However, this exchange process, which presumably takes place through a carbonate intermediate does not represent a redox process involved in net oxygen transport across the surface. The value of k_o reported in the table corresponds to the exchange mechanism and is not necessarily relevant to membrane operation. The rate of the reverse WGS reaction gives some indication of the rate of the redox process and its equivalent will be used in the future. An additional complication arising from the extremely rapid exchange is that the gas phase isotopic composition is not constant during the experiment. Therefore the nominal analysis based on a constant isotope fraction gives false values. The values indicated in the table for these experiments are limits based on the nominal values and a semiquantitative interpretation of the effects of the changing gas composition. A full simulation with a changing gas composition is required to obtain the best values of D_O and will be done during the next quarter.

(2) Transient oxygen isotope infusion in operating membrane reactors.

All the parts for the membrane reactor have been received and initial assembly and shakedown of the reactor is currently underway. As described in the previous report, the membrane reactor is a tubular design, rather than the initial design to use disc-shaped membranes. Tension is held on the seals by a bellows fitting at the end of the reactor. We have been delayed by the discovery this summer that the existing Hasteloy outer tube which forms part of our reactor system and which was to contain the membrane assembly had been distorted by improper mounting which resulted in bending by thermal expansion forces at high temperature. We received its replacement from the shop during August. Initial tubular samples of $La_{0.6}Sr_{0.4}Fe_{0.8}Co_{0.2}O_{3-x}$ have been received from Professor Jacobson's group during the past three months and will be the first materials tested in the reactor.

Progress during the last 3 months at UH

Electrical conductivity relaxation.

We have continued electrical conductivity relaxation measurements to obtain values of D and k to guide the infusion studies. The new apparatus has a much faster switching time (300msec). We are also using a lock-in amplifier ac technique in order to measure very small changes in the resistance of the sample. This method permits data acquisition over a wider range of pressure switches on the same sample and measurements with only small departures from equilibrium.

The specific compositions that have been measured are shown in the table. Of these, we will remeasure $La_{0.2}Sr_{0.8}FeO_{3-x}$ because of some discrepancies in the results and we will complete the measurements on $La_{0.2}Sr_{0.8}Fe_{0.8}Cr_{0.2}O_{3-x}$. The results for the four systems completed to date are shown in the figures below for both D and k

$La_{0.2}Sr_{0.8}FeO_{3-x}$
$La_{0.2}Sr_{0.8}Fe_{0.8}Cr_{0.2}O_{3-x}$
$La_{0.5}Sr_{0.5}FeO_{3-x}$
$La_{0.5}Sr_{0.5}Fe_{0.8}Ga_{0.2}O_{3-x}$
$La_{0.6}Sr_{0.4}Fe_{0.8}Co_{0.2}O_{3-x}$

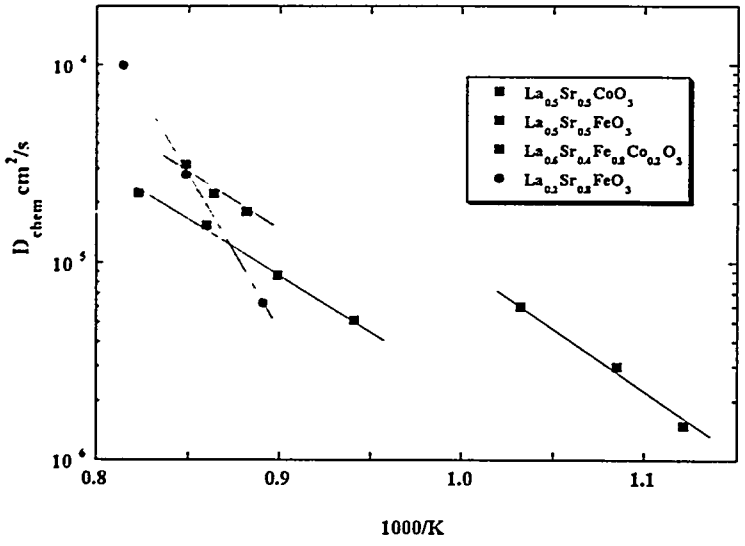

Figure 3 Comparison of D_{chem} values measured by electrical conductivity relaxation.

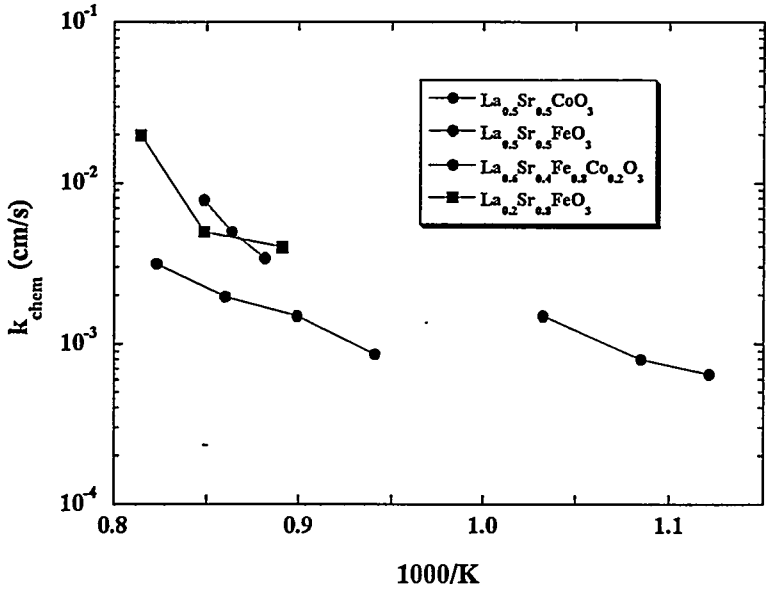

Figure 4 Comparison of k_{chem} values measured by electrical conductivity relaxation.

In both sets of data, the results for $La_{0.2}Sr_{0.8}FeO_{3-x}$ are anomalous and will be remeasured. The results show that the addition of cobalt increases both D and k relative to iron as anticipated from previous data

In order to carry out the isotope transient/membrane experiments at UT, we need to fabricate tubes of the appropriate dimensions. We will, for the present, use $La_{0.6}Sr_{0.4}Fe_{0.8}Co_{0.2}O_{3-x}$ as the material. We used the sintering protocol that we have developed to fabricate suitable rods. Attempts to machine the sintered rods to form tubes were not successful. Two alternatives were proposed. In the first, cold isostatic pressing is used to directly form the green tube, which is then sintered. Second, a green rod is partially sintered and then machined. We have evaluated the former route and found that it can be used successfully to make tubes of the appropriate dimensions. In the figure below is a representative example of a tube isostatically pressed and sintered is shown. The outside diameter is 6mm and the wall thickness is 0.5mm. Approximately 1 cm sections of this tube will be cut and mounted in the permeation apparatus at UT.

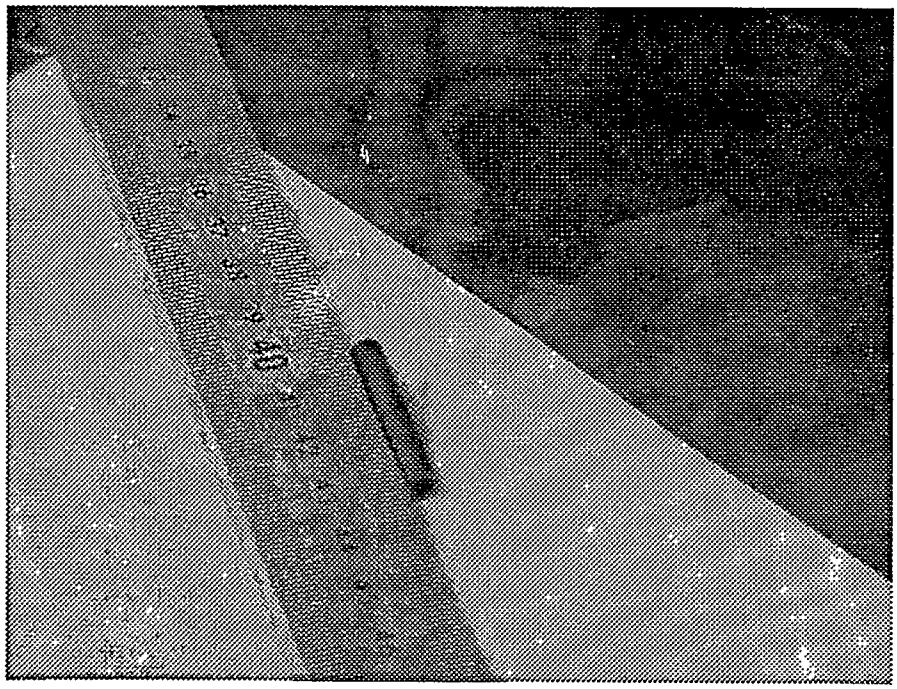

Fig. 5 Sintered tube of $La_{0.6}Sr_{0.4}Fe_{0.8}Co_{0.2}O_{3-x}$ for use in isotopic transient measurements.

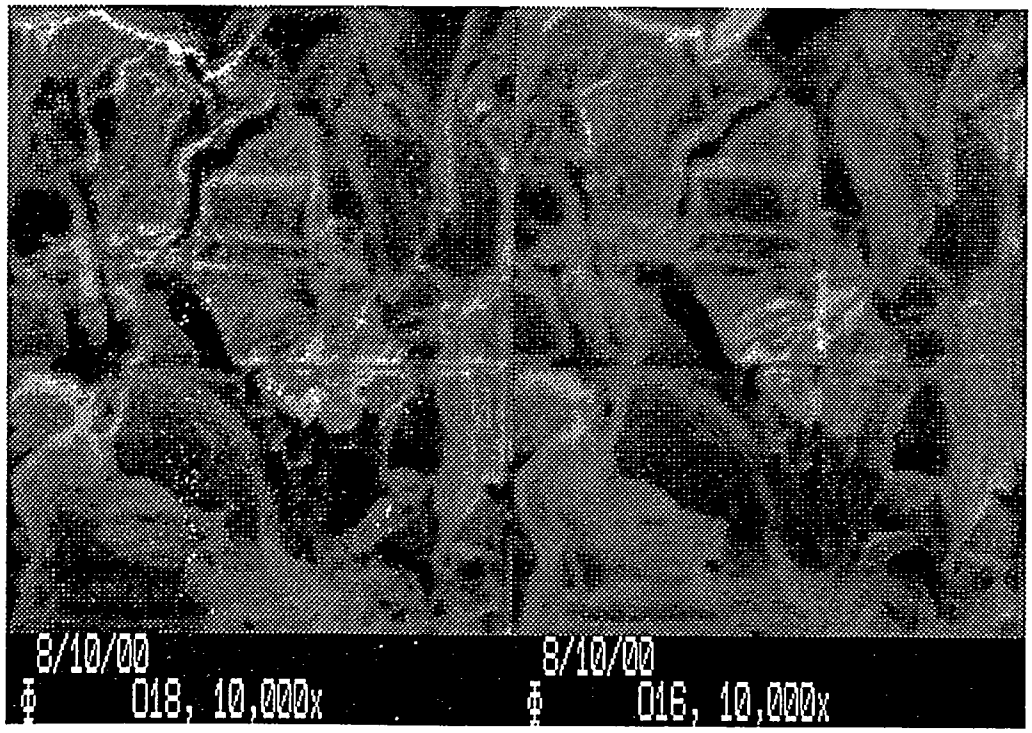

Fig 6 O18 and O16 SIMS images of a polyphasic ceramic to illustrate the resolution

The gallium source for the SIMS instrument has been delivered and installed. This gallium

source will provide higher resolution in-depth profiling than currently available. The software and resolution capability are being evaluated. The images below are the O16 and O18 images of a multiphase sample that was used as a reference for the resolution. The figures are 20 mm by 30 mm and indicate sub-micron resolution.

DOE Tasks for next 3 months University of Houston

(1) We will continue the electrical conductivity relaxation measurements on $La_{0.2}Sr_{0.8}FeO_3$ to resolve the observed anomaly and complete the measurements on $La_{0.2}Sr_{0.8}Fe_{0.8}Cr_{0.2}O_{3-x\square\square}$.
(2) Additional tubular and disk samples of $La_{0.2}Sr_{0.8}Cr_{0.2}O_{3-x}$ will be prepared for transient membrane studies and isotope infusion.
(3) The commissioning of gallium source for the SIMS instrument will be completed and used for higher resolution isotope depth profiles.
(4)

DOE Tasks for next 3 months University of Toronto.

(1) ^{18}O infusion in ferrites in gradientless conditions.

(a) The analysis of the profiles obtained in this quarter will be completed, including simulations with changing gas composition to obtain the best values of the transport parameters. One of the profiles also remains unmeasured (750°C reducing atmosphere infusion for in CO_2/H_2) and will be analyzed.

(b) Further examinations of the oxygen transport in $La_{0.2}Sr_{0.8}FeO_{3-x}$ and $La_{0.2}Sr_{0.8}Fe_{0.8}Cr_{0.2}O_{3-x}$ under reducing conditions will be performed. We will use C^*O_2/CO mixtures for the infusion, thus establishing a defined oxygen potential, but allowing measurement of the redox process by being able to follow the extent of isotopic equilibration between CO and CO_2 in the mass spectrometer.

(c) Additional infusions in air will be performed to extend the temperature range on the ferrites above and repeat several of the conditions.

(d) After these, time permitting, we will perform infusion measurements on an additional composition, either $\mathbf{La_{0.6}Sr_{0.4}Fe_{0.8}Co_{0.2}O_{3-x}}$ or $La_{0.6}Sr_{0.4}FeO_3$ at the standard conditions above.

(2) Operating membrane experiments

(a) The initial shake-down experiments will proceed as before. The initial assembly will use a dense alumina or quartz tube in place of the membrane. This will allow shakedown of the system without risking the perovskite tubes and proved rigorous leak-check to validate the seals. If all goes well, we will then start oxygen permeation measurements (with no reductant on the fuel side) towards the end of the period with the $\mathbf{La_{0.6}Sr_{0.4}Fe_{0.8}Co_{0.2}O_{3-x}}$ tube currently available.